

# On the Way Toward Understanding Solution Chemistry of Lithium Polysulfides for High Energy Li–S Redox Flow Batteries

Huilin Pan, Xiaoliang Wei, Wesley A. Henderson, Yuyan Shao, Junzheng Chen, Priyanka Bhattacharya, Jie Xiao,\* and Jun Liu\*

Lithium–sulfur (Li–S) redox flow battery (RFB) is a promising candidate for high energy large-scale energy storage application due to good solubility of long-chain polysulfide species and low cost of sulfur. Here, the fundamental understanding and control of lithium polysulfide chemistry are studied to enable the development of liquid phase Li–S redox flow prototype cells. These differ significantly from conventional static Li–S batteries targeting for vehicle electrification. A high solubility of the different lithium polysulfides generated at different depths of discharge and states of charge is required for a flow battery in order to take full advantage of the multiple electron transitions. A new dimethyl sulfoxide based electrolyte is proposed for Li–S RFBs, which not only enables the high solubility of lithium polysulfide species, especially for the short-chain species, but also results in excellent cycling with a high Coulombic efficiency. The challenges and opportunities for the Li–S redox flow concept have also been discussed in depth.

## 1. Introduction

Closely linked with the rapid development of energy harvesting from renewable energy sources such as wind and solar, low cost, high energy density and long lifespan large-scale energy storage has become critically important.<sup>[1]</sup> RFB is a promising technology for this purpose,<sup>[2]</sup> which provides for flexible operation, a long calendar life, easy scalability and potentially a low cost.<sup>[3]</sup> Sulfur is low cost and nontoxic with a high theoretical capacity (1675 mA h g<sup>-1</sup>) and energy density (≈2600 W h kg<sup>-1</sup>), thus propelling this active material to a position of paramount interest in recent years.<sup>[4]</sup> The long-chain polysulfides produced in a Li–S battery are highly soluble in the electrolyte, which could become advantageous for Li–S RFBs since the higher the solubility of the active species (i.e., Li<sub>2</sub>S<sub>x</sub>), the higher the

energy density of the RFB. The concept of Li–S RFBs can be found in patents<sup>[5]</sup> and publications using solid sulfur or dissolved lithium polysulfides as the starting cathode for Li–S batteries.<sup>[6]</sup> Recently, Li–S RFBs were demonstrated in static and semi-solid or suspension flow cells.<sup>[7,8]</sup> However, to extend this concept to true redox flow batteries, the charge/discharge processes of the polysulfides involve both electrochemical and chemical reactions need to be carefully controlled in particular related to the possibility of solid precipitation due to the insoluble short-chain polysulfides formed during long term cell cycling.<sup>[9]</sup> It is still worthwhile to explore the electrochemical conditions to enable a true liquid phase Li–S RFB.

For Li–S RFBs, the challenge is that the short-chain polysulfides, e.g., Li<sub>2</sub>S<sub>2</sub>, are generally insoluble in aprotic solvents, which hinders the high utilization rate of sulfur. The achievable energy density is critically dependent on the solubility, and on which polysulfide reaction (how many electrons) can be utilized (Table 1). In addition, the deposition of insoluble short-chain species onto the carbon current collector may further shorten the cell lifespan by blocking the flow channels. So far, there are few reports regarding a fundamental understanding of the solution chemistry of short-chain polysulfides or how to increase Li<sub>2</sub>S<sub>2</sub>/Li<sub>2</sub>S solubility, which is critical for enabling Li–S RFBs (see Table 1 for detailed information). In this work, a new type of DMSO-based electrolyte recipe is proposed, which enables both high solubility of lithium polysulfide species, especially for the short-chain species, and good cycling performance for Li–S RFBs.

## 2. Results and Discussion

### 2.1. Solution Chemistry of Lithium Polysulfide

Solubility is determined by the intrinsic properties and interactions between a given solute and solvent molecules.<sup>[10,11]</sup> It has been reported that the solvates present in an electrolyte with aprotic solvents are strongly related to the ionic association strength of the salt (i.e., the tendency for the anions to coordinate with the cations) and the structure of the solvent

Dr. H. Pan, Dr. X. Wei, Dr. Y. Shao, Dr. J. Chen,  
Dr. J. Xiao, Dr. J. Liu  
Joint Center for Energy Storage Research, USA  
Dr. H. Pan, Dr. X. Wei, Dr. W. A. Henderson,  
Dr. Y. Shao, Dr. J. Chen, Dr. P. Bhattacharya,  
Dr. J. Xiao, Dr. J. Liu  
Pacific Northwest National Laboratory  
Richland, WA 99352, USA  
E-mail: jie.xiao@pnnl.gov; jun.liu@pnnl.gov



DOI: 10.1002/aenm.201500113

**Table 1.** Calculation of energy density of Li–S flow battery with different concentration of S.

		$S_8^{2-} \rightarrow S_4^{2-}$	$S_8^{2-} \rightarrow S_2^{2-}$	$S_8^0 \rightarrow S_4^{2-}$	$S_8^0 \rightarrow S_2^{2-}$	$S_8^0 \rightarrow S^{2-}$
Capacity [Ah kg <sup>-1</sup> ]		209	627	418	836	1672
Voltage [V]		2.2	2	2.2	2	2
Energy (weight) density [W h kg <sup>-1</sup> ]		459	1254	919	1672	3344
	0.5 M	7	20	14	26	53
Volumetric	1 M	14	40	29	53	106
energy density	2 M	29	80	58	107	213
	5 M	73	125	147	214	534
[W h L <sup>-1</sup> ]	10 M	146	250	294	428	1068

Note: The concentration is based upon elemental S. Parasitic weight and volume were not included in the calculations.

molecules.<sup>[12–14]</sup> Understanding and controlling the properties of the solute and solvent may therefore provide new clues to improve the solubility of Li<sub>2</sub>S<sub>x</sub> species.<sup>[15,16]</sup> Methods to increase the solubility of polysulfides, especially for short-chain species like Li<sub>2</sub>S<sub>2</sub>, have not been reported before and will be discussed in detail below.

In general, the dielectric constant of the solvent provides a rough evaluation of a solvent's polarity, which can be considered to be the ability of a specific solvent to reduce/dissociate the solute's effective internal charge. Thus, a higher dielectric constant of a solvent generally means a higher solubility of a solute.<sup>[11]</sup> Furthermore, the molecular polarity of the solvent is also directly related to the dipole moment of solvent,<sup>[17]</sup> which is the heart of intermolecular attraction. Three types of solvents—DMSO, THF, and a DOL:DME—with different polarity properties (Table S1, Supporting Information) are compared. The DOL:DME (1:1, v:v) mixture<sup>[18]</sup> is often used for static Li–S batteries and is used as a reference here. The polarity of these three solvents follows the order of DMSO > THF > DOL:DME. It was reported earlier that both DMSO and THF have high solubility for long-chain polysulfides, e.g., Li<sub>2</sub>S<sub>8</sub>,<sup>[19]</sup> consistent with the polarity trend in Table S1, Supporting Information. However, the solubility of short-chain species (e.g., Li<sub>2</sub>S<sub>2</sub>) in aprotic solvents, which is even more critical for RFBs with liquid catholytes, is largely unknown.

Figure 1a shows the solubility of Li<sub>2</sub>S<sub>x</sub> species (1 < x ≤ 8) in the solvents noted above. DMSO with the highest polarity exhibits the highest solubility for the Li<sub>2</sub>S<sub>x</sub> species among these three solvents, with a sequence of DMSO > THF > DOL:DME. These three solvents all exhibit high solubility for the Li<sub>2</sub>S<sub>8</sub>. However, the solubility of the Li<sub>2</sub>S<sub>x</sub> species in all of the solvents drops sharply with decreasing polysulfide chain length. For example, the solubility of the Li<sub>2</sub>S<sub>6</sub> composition is only half that of Li<sub>2</sub>S<sub>8</sub>, or lower. This is consistent with the computational results that short-chain Li<sub>2</sub>S<sub>x</sub> species (x < 6) have poor solubility because they prefer to form dimer Li<sub>4</sub>S<sub>2x</sub> composite.<sup>[20]</sup> Especially, in the DOL:DME mixed solvents, the solubility of the short-chain polysulfides drops much faster than for the other two solvents. For the Li<sub>2</sub>S<sub>4</sub> composition, the solubility is less than 0.1 M in DOL:DME. To fully take advantage of the Li–S redox flow cell design, a high solubility is necessary from the starting Li<sub>2</sub>S<sub>8</sub> catholyte to the end species such as Li<sub>2</sub>S<sub>2</sub>/Li<sub>2</sub>S.

From this point of view, DMSO is the preferred solvent for Li–S RFBs (Figure 1a).

As mentioned earlier, the solubility is an intrinsic property of both the solute and solvent, which is determined by the intermolecular interactions between the two.<sup>[11]</sup> An alternative method to adjust the intermolecular forces and solvating effects is to introduce complex-forming anion ligands into the liquids.<sup>[13,15]</sup> The solubility of the original solute becomes tunable in the presence of anions with differing ionic association strengths. It has been reported that ionic association strength of anions in acetonitrile (AN)<sub>n</sub>-LiX (where X represents the anion) electrolytes increases in the order: LiPF<sub>6</sub> < LiTFSI ≤ LiClO<sub>4</sub> < LiBF<sub>4</sub> < LiCF<sub>3</sub>SO<sub>3</sub> (LiTf).<sup>[14]</sup> Two anions, TFSI<sup>-</sup> and Tf<sup>-</sup>, with rather different ionic association strength, were therefore introduced into DMSO- and THF-based solutions to explore the anions' effects on the solubility of Li<sub>2</sub>S<sub>x</sub> species (Figure 1b). The mole ratios of solvent versus salt (LiTFSI or LiTf) were tuned in Figure 1b to optimize the additive content. Compared to the pure THF or DMSO solvent, the addition of even a small amount of LiTFSI or LiTf (solvent/salt ratio = 30) significantly increases the Li<sub>2</sub>S<sub>2</sub> solubility, indicating that the anions do affect the interaction force between Li<sup>+</sup> cations and the S<sub>x</sub><sup>2-</sup> anions in the mixtures for both DMSO and THF solvents. This anion effect can also be found in aqueous system, in which the addition of Cl<sup>-</sup> anion into vanadium sulfate solutions stabilizes and improves the solubility for vanadium ions.<sup>[21]</sup> LiTf, with higher ionic association strength, is more effective than LiTFSI at increasing the solubility of Li<sub>2</sub>S<sub>2</sub> in both THF and DMSO (blue and black curves in Figure 1b). However, further increasing the LiTf content in the solvents leads to slight decrease in the Li<sub>2</sub>S<sub>2</sub> solubility in both cases. LiTFSI (red curve in Figure 1b) also improves the dissolution of Li<sub>2</sub>S<sub>2</sub>, but the solubility increase is limited due to the weaker ionic association strength of LiTFSI as compared to that in LiTf. The highest solubility increase of Li<sub>2</sub>S<sub>2</sub> is observed in DMSO with LiTf addition. Figure 1c further compares the Li<sub>2</sub>S<sub>2</sub> solubility by tailoring the LiTf concentrations. An optimized DMSO:LiTf ratio of 30, corresponding to ≈0.5 M LiTf in DMSO, is identified, which contributes to an almost ten fold increase in the Li<sub>2</sub>S<sub>2</sub> solubility relative to the pure DMSO solvent. The viscosity and solubility are well balanced at this optimized ratio, making this DMSO<sub>30</sub>:LiTf composition promising for high energy Li–S RFBs.

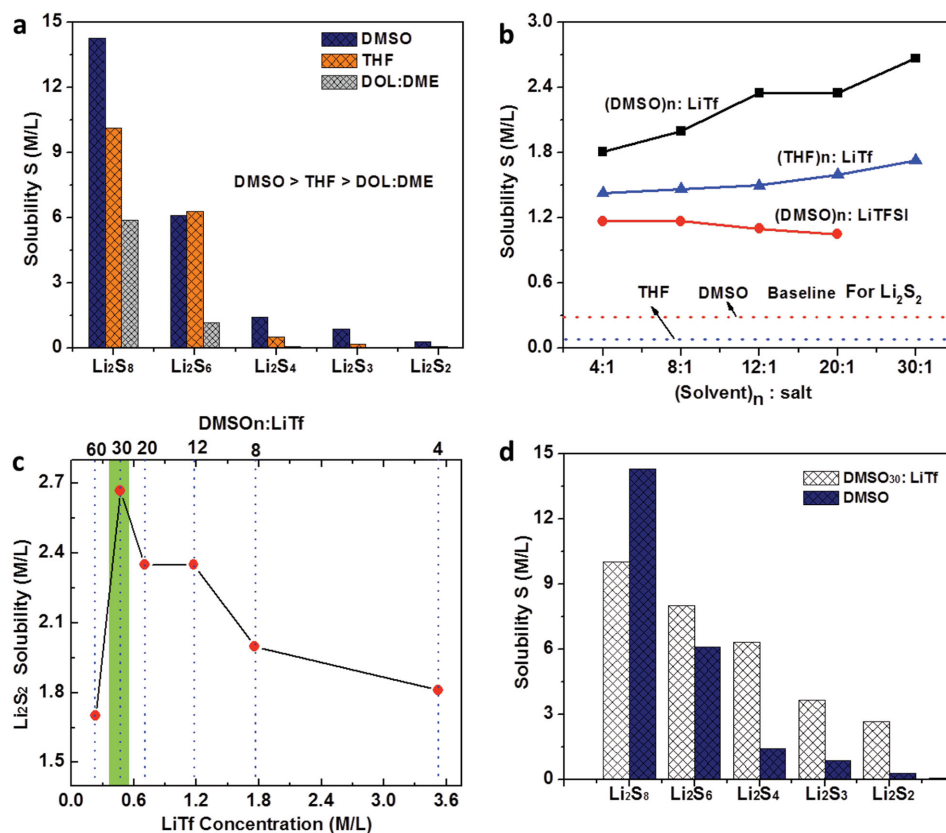


**Figure 1.** The solubility study. a) The solubility of  $\text{Li}_2\text{S}_x$  in pure solvents /mixed solvents. b) The solubility of  $\text{Li}_2\text{S}_2$  in DMSO or THF solvents with the addition of complex-forming anions, LiTFSI or LiTf. c) The effect of the additive concentration of LiTf on solubility of  $\text{Li}_2\text{S}_2$ . d) The solubility comparison of  $\text{Li}_2\text{S}_x$  in DMSO:LiTf and DMSO solvents. Note that the concentration is based on elemental S.

Other polysulfide  $\text{Li}_2\text{S}_x$  species ( $x = 6, 4, 3,$  and  $2$ ) also have a significant solubility increase in this  $\text{DMSO}_{30}$ :LiTf recipe (Figure 1d), except for  $\text{Li}_2\text{S}_8$  which displays a lower solubility than for the pure solvent. UV-vis spectra of  $\text{Li}_2\text{S}_x$  in DMSO and  $\text{DMSO}_n$ :LiTf mixtures were then conducted to understand the interaction changes between the  $\text{Li}^+$  cations and different  $\text{S}_x^{2-}$  anions after incorporating LiTf (Figure S1, Supporting Information).  $\text{Li}_2\text{S}_8$  exhibits similar UV-vis spectra in both pure DMSO and  $\text{DMSO}_{30}$ :LiTf (Figure S1a, Supporting Information), indicating that LiTf does not change the equilibria much for the long-chain species which is consistent with the high  $\text{Li}_2\text{S}_8$  solubility both before and after the addition of LiTf (Figure 1d). In contrast, UV-vis spectra of solutions with short-chain  $\text{Li}_2\text{S}_2$  in DMSO dramatically alter after the addition of LiTf (Figure S1b, Supporting Information), in agreement with the large solubility change of  $\text{Li}_2\text{S}_2$ . It seems that the anion effect plays a more important role for the originally insoluble short-chain species, which is worth further study.

To further understand how the different ions interact with each other in the presence of the triflate anion ( $\text{Tf}^-$ ), Raman spectra were performed for  $\text{DMSO}_n$ :LiTf solutions with and without  $\text{Li}_2\text{S}_2$  (Figure 2a). The first peaks of interest are from the vibrational mode of C-S-C in DMSO ( $668.2$  and  $697.8\text{ cm}^{-1}$ ).<sup>[22]</sup> There is no visible Raman shift of  $\nu(\text{C-S-C})$  before and after the addition of  $\text{Li}_2\text{S}_2$ , indicating that DMSO itself has weak interaction with  $\text{Li}_2\text{S}_2$ . This is consistent with the low solubility

of  $\text{Li}_2\text{S}_2$  in pure DMSO solvent (Figure 1a). After adding LiTf in the electrolyte, a more important peak located at  $\approx 1040\text{ cm}^{-1}$  shows up and corresponds to the vibration of  $\nu(\text{SO}_3)$  in  $\text{Tf}^-$  anions. This peak is very sensitive to its surrounding chemical environment<sup>[23]</sup> and enlarged in Figure 2c (red line). Although there is a slight overlap with the Raman peak assigned to  $\text{S}=\text{O}$  ( $1045\text{ cm}^{-1}$ ) in DMSO,<sup>[24]</sup> a closer inspection identifies the peak at  $1033\text{ cm}^{-1}$  belonging to the free  $\text{Tf}^-$  anions which is labeled in Figure 2c (red). When free  $\text{Tf}^-$  forms ion contact pairs or aggregates, the  $\text{Tf}^-$  original peak will shift to a higher value. The higher grade of ionic aggregate, the larger shift of this Raman frequency.<sup>[23]</sup> When  $\text{Li}_2\text{S}_2$  is added into  $\text{DMSO}_{30}$ :LiTf, significant peak shift is seen (from red line to blue line in Figure 2b). A dominant peak occurs at  $1062\text{ cm}^{-1}$ , indicating the formation of high grade of ionic aggregates in the  $\text{DMSO}_{30}$ :LiTf- $\text{Li}_2\text{S}_2$  solution. That is, two or more  $\text{Li}^+$  cations are contacting simultaneously with one  $\text{Tf}^-$  anion. Since  $\text{Li}^+/\text{Tf}^-$  ratio for LiTf itself is 1, the extra coordinated  $\text{Li}^+$  cations with  $\text{Tf}^-$  anions have to be supplied by  $\text{Li}_2\text{S}_x$ . The end result is the increase of solubility of  $\text{Li}_2\text{S}_2$  after the addition of LiTf. The Raman spectra of  $\text{DMSO}_n$ :LiTf- $\text{Li}_2\text{S}_2$  with other concentrations of LiTf are also performed, where ionic aggregates are still the dominant species thus  $\text{Tf}^-$  anion works similarly to enhance the solubility of  $\text{Li}_2\text{S}_2$  by coordinating with  $\text{Li}^+$  from  $\text{Li}_2\text{S}_x$  (Figure S2, Supporting Information). In addition, high polar DMSO solvent might also facilitate forming aggregates in  $\text{DMSO}_n$ :LiTf- $\text{Li}_2\text{S}_2$

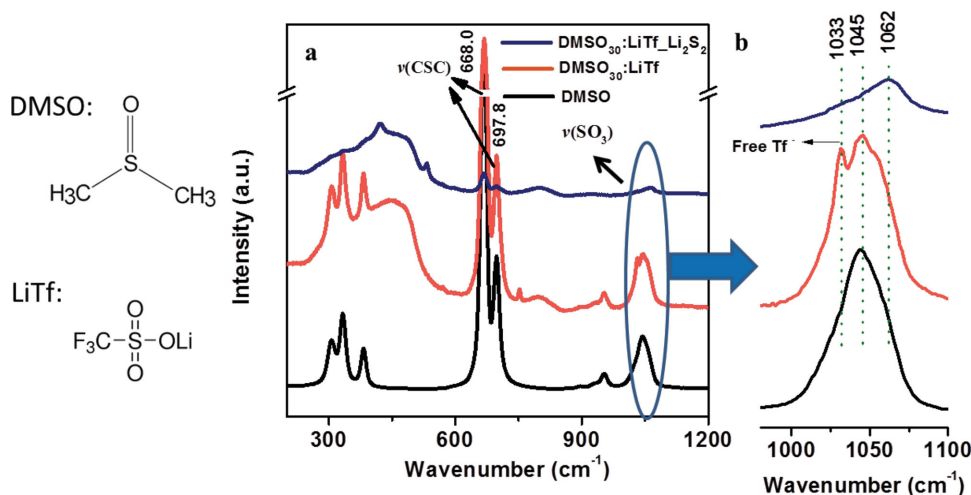


**Figure 2.** The molecular structure of DMSO and LiTf and a) Raman spectra for DMSO<sub>30</sub>:LiTf with and without Li<sub>2</sub>S<sub>2</sub>. Enlarged Raman spectra for  $\nu(\text{SO}_3)$  from LiTf in DMSO<sub>30</sub>:LiTf with and without Li<sub>2</sub>S<sub>2</sub> dissolution, respectively.

composite. This also somehow explains why LiTf addition in DMSO is more effective in increasing the solubility of Li<sub>2</sub>S<sub>2</sub> than THF solvent (Figure 1b).

## 2.2. Li-S Redox Flow Batteries

Based on the findings discussed above, a catholyte was prepared by dissolving 1 M Li<sub>2</sub>S<sub>8</sub> in DMSO<sub>30</sub>:LiTf in the presence

of 1 M LiTFSI as the supporting salt. This catholyte was initially tested in a nonflowing static cell (Figure 3a,b). During the first cycle, the dissolved Li<sub>2</sub>S<sub>x</sub> could deliver a high reversible capacity of 1450 mA h g<sup>-1</sup> S at C/5, indicating a high utilization of the sulfur due to its availability in the phase. The deposition of insoluble and insulating Li<sub>2</sub>S<sub>2</sub>/Li<sub>2</sub>S species is largely reduced in this electrolyte. However, large fluctuations appear during the charge step after a few cycles, which is believed to be due to the incompatibility between DMSO and the Li metal anode

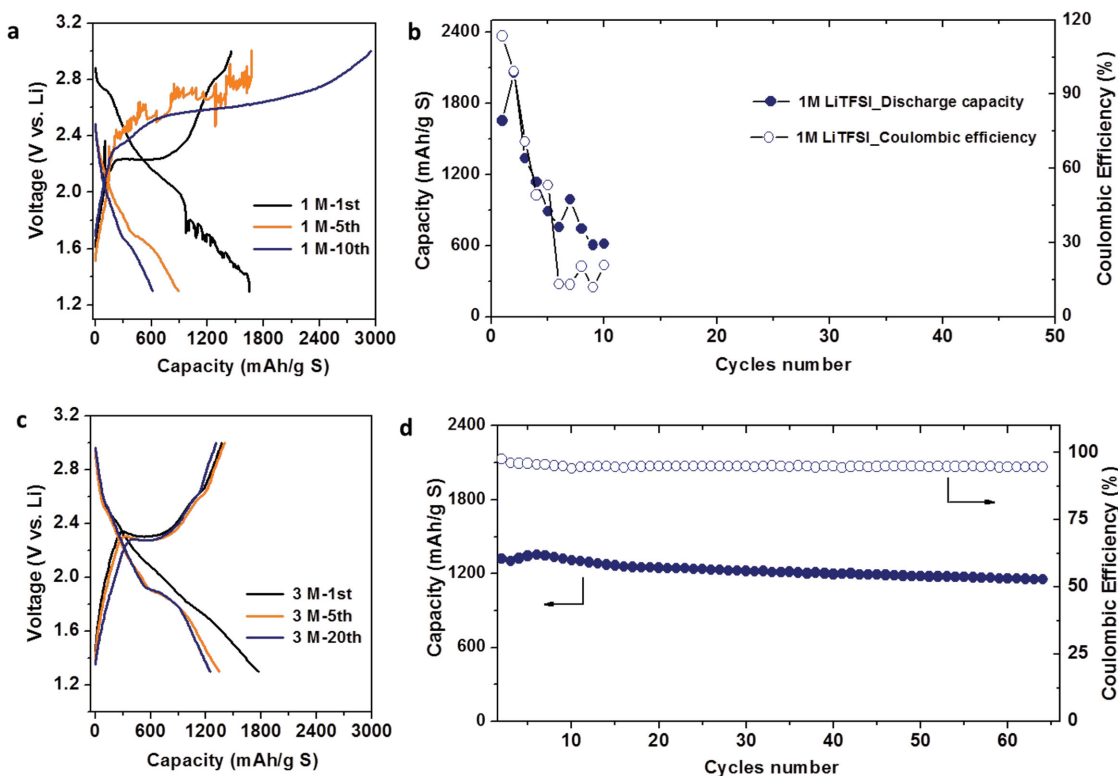


**Figure 3.** The charge/discharge curves and cyclic performance of dissolved Li<sub>2</sub>S<sub>8</sub> in DMSO<sub>30</sub>:LiTf new “solvent” with a,b) 1 M LiTFSI and c,d) 3 M LiTFSI as supporting salt at a current rate of C/5. Note: Capacity is based on S.

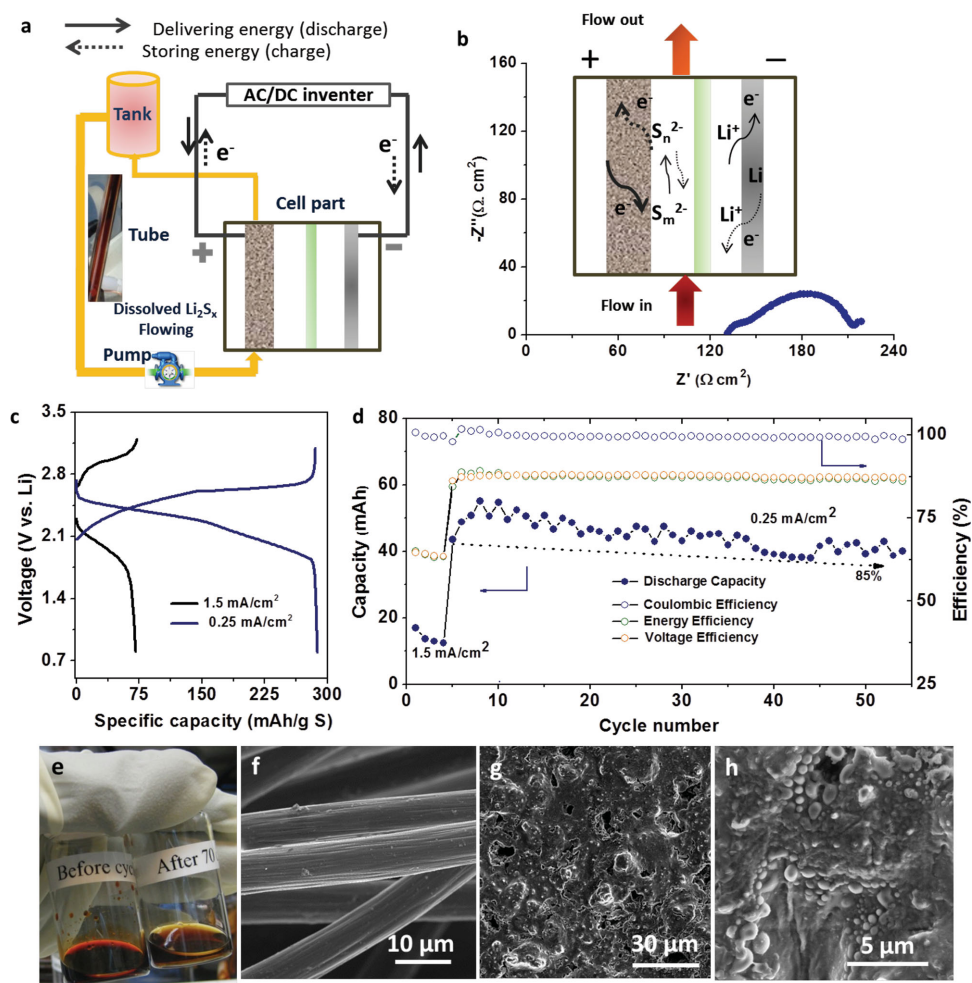


**Figure 4.** The demonstration of Li-S RFB using DMSO<sub>30</sub>:LiTf electrolyte recipe, with 3 M LiTFSI as supporting salt. a) Configuration of Li-S redox flow battery. 40 cm<sup>2</sup> carbon felt, polyethylene polymer film and fresh Li as cathode current collector, separator and counter electrodes, respectively. 15 mL completely dissolved Li<sub>2</sub>S<sub>x</sub> flows into/out the cell part and the redox reaction takes place under a continuous flowing model at a rate of 40 mL min<sup>-1</sup>. b) The electrochemical impedance of overall Li-S redox flow cell at OCV state; the inset is the scheme of main cell part for flow battery. c) Charge/discharge curves and d) cyclic performance and efficiency of Li-S RFB at different current densities. e) The images for the catholyte for Li-S RFB before and after cycling. f-h) SEM images of carbon felt and Li anode after 70 cycles.

as reported before.<sup>[25]</sup> Therefore, fast capacity fading and a low Coulombic efficiency were observed. To address this problem, the concentration of the supporting salt LiTFSI was increased to 3 M to reduce the side reaction between the uncoordinated free DMSO solvent molecules and the lithium anode. Interestingly, the Coulombic efficiency of the DMSO-based Li-S cell with this concentrated electrolyte was greatly increased to 95% without the use of LiNO<sub>3</sub> as an additive.<sup>[26]</sup> The cycling stability was also significantly improved (Figure 3c,d). (Note that the charge/discharge curves are slightly different from those in DOL:DME co-solvents due to the impact of solvation effect of solvent.<sup>[27]</sup>) A stable capacity of  $\approx 1200$  mA h g<sup>-1</sup> S can be delivered at C/5 with capacity retention of 87% of the second cycle after 65 cycles. This indicates that decreasing the amount of “free” DMSO solvent molecules not only mitigates the corrosion on Li anode side, but also slows down the shuttle reaction of Li<sub>2</sub>S<sub>x</sub>.<sup>[28–30,25]</sup> To our knowledge, this is the first demonstration that DMSO, usually incompatible with the Li metal anode,

can be successfully used to enable high energy Li-S cells with a stable cyclic ability and high Coulombic efficiency. The test shows high S utilization, good reversibility, high Coulombic efficiency, and slight capacity fading as compared to previous reports.

The electrolyte concept was then further validated in a real Li-S redox flow configuration. The configuration of the real continuous flow battery is more complicated than button cells and consists of a main cell compartment, external pump, tank and connecting tubes (Figure 4a). The results from Figure 4 also show how much more difficult it is to make a real redox flow cell work than a static cell. The viscosity and the concentration of catholyte need to be tuned step by step to balance the flow rate and maximize the capability of the whole system. For example, each different electrolyte recipe with fixed viscosity and concentration, different flowing rate ranging from 20 to 80 mL min<sup>-1</sup> at a relatively low current density (0.25 mA cm<sup>-2</sup>) will be applied to identify the optimized flow rate at which the

reversible capacity reaches maximum. Based on the optimized combination of catholyte concentration and flow rate, different current densities will be further applied to evaluate the power/energy ratio for practical applications. At the same time, the architecture of the current collector will also be modified to provide more reactive sites for polysulfides without impeding the smooth flowing of catholyte. Therefore, based upon the solubility of the  $\text{Li}_2\text{S}_2$  measured in Figure 1b,c, the concentration of the starting long-chain  $\text{Li}_2\text{S}_8$  catholyte was reduced to 0.4 M to avoid or alleviate the potential deposition of the insoluble  $\text{Li}_2\text{S}_2/\text{Li}_2\text{S}$  that may block the reaction sites on the carbon felt current collector. The overall resistance of the flow cell at OCV state was around  $130 \Omega \text{ cm}^2$  (Figure 4b), higher than that of an aqueous vanadium RFB ( $\approx 2.5 \Omega \text{ cm}^2$ ),<sup>[31]</sup> due to the relatively low conductivity of the organic electrolyte.

Figure 4c shows the charge/discharge curves of the flow battery at two different current densities. At a high current density of  $1.5 \text{ mA cm}^{-2}$  (60 mA in total), only a small specific capacity of  $71 \text{ mA h g}^{-1}$  (based on S mass) can be delivered with a huge polarization of  $\approx 0.7 \text{ V}$ , indicating the poor reaction kinetics of the nonaqueous catholyte at high current density. The low surface area ( $0.3 \text{ m}^2 \text{ g}^{-1}$  for the carbon felt used), i.e., limited reaction sites of the current collector, also influenced the completion of sulfur reaction. After switching to a reduced current density of  $0.25 \text{ mA cm}^{-2}$  (10 mA in total), however, a specific capacity of  $\approx 280 \text{ mA h g}^{-1}$  S was obtained along with a much lower polarization. This capacity is about four times higher than that at  $1.5 \text{ mA cm}^{-2}$  and almost equals to the capacity contribution from the first discharge plateau in a static cell (Figure 3c). The length of the second plateau in static cells is directly related to the surface area of the carbon hosts in the composite C–S cathode.<sup>[32]</sup> Considering the low surface area of the carbon felt, it is understandable that the second plateau almost disappeared. From this point of view, the design of the current collector needs further modification to provide sufficient reaction sites for polysulfides before they diffuse out. Additionally, the viscosity of the catholyte plays an important role in the cell performance that needs further consideration. However, the capacity retention from this preliminary study for this continuous-flowing Li–S cell remains high at  $\approx 85\%$  after more than 50 cycles (Figure 4d), indicating that the selection of electrolyte recipe is indeed very critical to develop this new technology.

During cycling, the  $\text{Li}_2\text{S}_x$  catholyte remains a clear solution indicating the successful prevention of insoluble short-chain polysulfide deposition in the tailored DMSO-based electrolyte (Figure 4e). Nor is there obvious precipitation of insoluble species on the cycled carbon felt (Figure 4f), further confirming the effectiveness of this new electrolyte recipe for Li–S flow cells. Of note, the Coulombic efficiency of the flow cell is extremely high (close to 100%) in the absence of a  $\text{LiNO}_3$  additive suggesting the decrease or elimination of the “shuttle” reactions in this electrolyte. The interface compatibility between Li metal and the solvent is also largely improved, as confirmed by SEM images showing a smooth anode surface after cycling. No sharp Li dendrites is observed (Figure 4g). Instead, a closer inspection (Figure 4h) reveals that spherical Li particles redeposited on the anode after cycling, which may provide new information related to Li anode protection work. Furthermore, the flow cell with this new DMSO-based electrolyte exhibits high

energy, voltage and Coulombic efficiencies of 87%, 87%, and 99.5%, respectively (Figure 4d), all of which are critical for the practical utilization of RFBs. It is noticeable that the Coulombic efficiency of the flow Li–S cell is much higher than that for the comparable static cell (Figure 3d). One explanation for this is that the flowing condition on the anode side reduces the concentration gradient of  $\text{Li}^+$  cations in the vicinity of the Li surface during deposition, thus mitigating the formation of detrimental Li dendrites which may become “dead” Li.<sup>[33]</sup> Future work will focus on the modulation of the electrolyte viscosity of the catholyte with dissolved  $\text{Li}_2\text{S}_x$ , as well as the rational design of current collector structures to take full advantage of the high energy density of Li–S RFBs.

### 3. Conclusion

The factors that govern the solubility of the polysulfide species in the catholyte of Li–S flow cells are discussed in this work. Fundamental details regarding the basic solution chemistry of polysulfides in organic electrolytes have been carefully investigated. DMSO has been selected as the appropriate solvent for the Li–S redox flow system because of its improved solubility of  $\text{Li}_2\text{S}_2$  relative to other solvents. The strong ionic association strength of the  $\text{TF}^-$  anion was used to further improve the  $\text{Li}_2\text{S}_x$  solubility by forming ionic aggregates, which then becomes soluble in the solution and beneficial to the practical application of the Li–S flow cells. To address the incompatibility of DMSO with Li metal, the concentration of the supporting salt ( $\text{LiTFSI}$ ) was increased to 3 M which stabilized the interface between the electrolyte and the anode surface. A high Coulombic efficiency and excellent capacity retention have been demonstrated here, for the first time, in a continuous flowing Li–S cell without the obvious formation of insoluble short-chain lithium polysulfide species which might interfere with the catholyte flow or block the reaction sites on the porous current collector. This work successfully correlates the fundamental solution chemistry to the final electrochemical performance of redox flow batteries thus providing important guidance for Li–S flow battery research and development.

### 4. Experimental Section

Dimethyl sulfoxide (DMSO, Sigma-Aldrich) and tetrahydrofuran (THF, Sigma-Aldrich) are used after 12 h drying by molecular sieves in a glove box. 1,3-Dioxolane (DOL, BASF) and dimethyl ether (DME, BASF) solvents are used as received. Lithium bis(trifluoromethanesulfonyl)imide ( $\text{LiN}(\text{SO}_2\text{CF}_3)_2$ ,  $\text{LiTFSI}$ , BASF) and lithium trifluoromethanesulfonate ( $\text{LiCF}_3\text{SO}_3$ ,  $\text{LiTf}$ , BASF) salts are used as received. Nominal  $\text{Li}_2\text{S}_x$  solutions are obtained by mixing stoichiometric  $\text{Li}_2\text{S}$  and  $\text{S}_8$  and stirring at  $60 \text{ }^\circ\text{C}$  in oil bath for 1–10 h inside the glove box. Solubility was obtained by first adding extra amount of stoichiometric  $\text{Li}_2\text{S}_x$  and followed by diluting the saturated solution gradually every 10 h until all species were dissolved. Raman spectra were collected on LabRAM Confocal Raman Microscope with 532 nm excitation laser. UV–vis spectra were performed by using UV-VIS-NIR Spectrophotometer (Shimadzu UV 3600).

Graphene was mixed with Polytetrafluoroethylene (PTFE) binder at a weight ratio of 95:5 to obtain carbon current collector. Static cells were assembled using graphene/PTFE film as cathode current collector, 1 M  $\text{Li}_2\text{S}_8$  dissolved into identified  $\text{DMSO}_{30}:\text{LiTf}$  recipe in presence of 1 and

3 M LiTFSI as electrolyte, Celgard film (3501) as separator and Li anode as a counter electrode. The flow cell was assembled with 40 cm<sup>2</sup> carbon felt (0.3 m<sup>2</sup> g<sup>-1</sup>) as a porous cathode current collector, 15 mL of 0.4 M Li<sub>2</sub>S<sub>8</sub> dissolved into the DMSO<sub>30</sub>:LiTf recipe with 3 M concentrated LiTFSI as catholyte, polyethylene polymer film as separator and fresh Li foil as anode, respectively. The charge/discharge was performed on LANHE tester. The electrochemical impedance for flow cell was tested at OCV state by Solartron Electrochemical Interface (Solartron SI 1287). The frequency range for electrochemical impedance spectra is 10 m–4 M Hz and the amplitude is 10 mV. A flow rate of catholyte solution was set at 40 mL min<sup>-1</sup>; a current density of 0.25–1.50 mA cm<sup>-2</sup> (10–60 mA in total) was used for the flow cell.

## Supporting Information

Supporting Information is available from the Wiley Online Library or from the author.

## Acknowledgments

This work was supported as part of the Joint Center for Energy Storage Research, an Energy Innovation Hub funded by the U.S. Department of Energy, Office of Science, Basic Energy Sciences. The Raman and SEM analyses were performed in the Environmental Molecular Sciences Laboratory, a national scientific user facility sponsored by the U.S. Department of Energy's Office of Biological and Environmental Research and located at Pacific Northwest National Laboratory (PNNL).

Received: January 15, 2015

Revised: March 7, 2015

Published online:

- [1] a) J. Liu, J.-G. Zhang, Z. Yang, J. P. Lemmon, C. Imhoff, G. L. Graff, L. Li, J. Hu, C. Wang, J. Xiao, G. Xia, V. V. Viswanathan, S. Baskaran, V. Sprenkle, X. Li, Y. Shao, B. Schwenzer, *Adv. Funct. Mater.* **2013**, *23*, 929; b) H. Pan, Y.-S. Hu, L. Chen, *Energy Environ. Sci.* **2013**, *6*, 2338.
- [2] a) K. C. Divya, J. Østergaard, *Electr. Power Syst. Res.* **2009**, *79*, 511; b) B. Dunn, H. Kamath, J.-M. Tarascon, *Science* **2011**, *334*, 928.
- [3] W. Wang, Q. Luo, B. Li, X. Wei, L. Li, Z. Yang, *Adv. Funct. Mater.* **2013**, *23*, 970.
- [4] a) X. Ji, K. T. Lee, L. F. Nazar, *Nat. Mater.* **2009**, *8*, 500; b) P. G. Bruce, S. A. Freunberger, L. J. Hardwick, J.-M. Tarascon, *Nat. Mater.* **2012**, *11*, 19; c) B. Scrosati, J. Garche, *J. Power Sources* **2010**, *195*, 2419; d) A. Manthiram, Y. Fu, S.-H. Chung, C. Zu, Y.-S. Su, *Chem. Rev.* **2014**; e) G. Xu, B. Ding, J. Pan, P. Nie, L. Shen, X. Zhang, *J. Mater. Chem. A* **2014**, *2*, 12662.
- [5] a) L. C. Jonghe, D. J. Visco, Y. S. Nimon, B. D. Katz, US Patent US8758914 B2, **2011**; b) J. Xiao, J. Zhang, G. L. Graff, J. Liu, W. Wang, J. Zheng, W. Xu, Y. Shao, Z. Yang, US Patent 20130260204, **2012**; c) J. Xiao, J. Liu, H. Pan, W. A. Henderson, US Patent 14/530,442, **2014**.
- [6] a) Y. Fu, Y.-S. Su, A. Manthiram, *Angew. Chem.* **2013**, *125*, 7068; b) R. D. Rauh, K. M. Abraham, G. F. Pearson, J. K. Surprenant, S. B. Brummer, *J. Electrochem. Soc.* **1979**, *126*, 523; c) G. Xu, B. Ding, P. Nie, L. Shen, J. Wang, X. Zhang, *Chem. Eur. J.* **2013**, *19*, 12306; d) G. Xu, B. Ding, P. Nie, L. Shen, H. Dou, X. Zhang, *ACS Appl. Mater. Interfaces* **2014**, *6*, 194.
- [7] F. Y. Fan, W. H. Woodford, Z. Li, N. Baram, K. C. Smith, A. Helal, G. H. McKinley, W. C. Carter, Y.-M. Chiang, *Nano Lett.* **2014**, *14*, 2210.
- [8] H. Chen, Q. Zou, Z. Liang, H. Liu, Q. Li, Y.-C. Lu, *Nat. Commun.* **2015**, *6*, 5877.
- [9] a) S. Walus, C. Barchasz, J.-F. Colin, J.-F. Martin, E. Elkaim, J.-C. Lepretre, F. Alloin, *Chem. Commun.* **2013**, *49*, 7899; b) M. A. Lowe, J. Gao, H. D. Abruna, *RSC Adv.* **2014**, *4*, 18347.
- [10] J. Burke, *Solubility Parameters: Theory and Application*, Vol. 3, CoOLConservation, **1984**.
- [11] Y. Chernyak, *J. Chem. Eng. Data* **2006**, *51*, 416.
- [12] W. A. Henderson, N. R. Brooks, W. W. Brennessel, V. G. Young, *J. Phys. Chem. A* **2003**, *108*, 225.
- [13] W. A. Henderson, F. McKenna, M. A. Khan, N. R. Brooks, V. G. Young, R. Frech, *Chem. Mater.* **2005**, *17*, 2284.
- [14] a) W. A. Henderson, *J. Phys. Chem. B* **2006**, *110*, 13177; b) D. M. Seo, O. Borodin, D. Balogh, M. O'Connell, Q. Ly, S.-D. Han, S. Passerini, W. A. Henderson, *J. Electrochem. Soc.* **2013**, *160*, A1061.
- [15] a) K. Ueno, J.-W. Park, A. Yamazaki, T. Mandai, N. Tachikawa, K. Dokko, M. Watanabe, *J. Phys. Chem. C* **2013**, *117*, 20509; b) J.-W. Park, K. Ueno, N. Tachikawa, K. Dokko, M. Watanabe, *J. Phys. Chem. C* **2013**, *117*, 20531.
- [16] a) J.-W. Park, K. Yamauchi, E. Takashima, N. Tachikawa, K. Ueno, K. Dokko, M. Watanabe, *J. Phys. Chem. C* **2013**, *117*, 4431; b) C. Zhang, A. Yamazaki, J. Murai, J.-W. Park, T. Mandai, K. Ueno, K. Dokko, M. Watanabe, *J. Phys. Chem. C* **2014**, *118*, 17362.
- [17] L. Onsager, *J. Am. Chem. Soc.* **1936**, *58*, 1486.
- [18] a) M.-Y. Chu, L. C. D. Jonghe, S. J. Visco, B. D. Katz, US Patent 6030720, **2000**; b) M. Hagen, P. Schiffels, M. Hammer, S. Dorfler, J. Tubke, M. J. Hoffmann, H. Althues, S. Kaskel, *J. Electrochem. Soc.* **2013**, *160*, A1205.
- [19] R. D. Rauh, F. S. Shuker, J. M. Marston, S. B. Brummer, *J. Inorg. Nucl. Chem.* **1977**, *39*, 1761.
- [20] M. Vijayakumar, N. Govind, E. Walter, S. D. Burton, A. Shukla, A. Devaraj, J. Xiao, J. Liu, C. Wang, A. Karim, S. Thevuthasan, *Phys. Chem. Chem. Phys.* **2014**, *16*, 10923.
- [21] L. Li, S. Kim, W. Wang, M. Vijayakumar, Z. Nie, B. Chen, J. Zhang, G. Xia, J. Hu, G. Graff, J. Liu, Z. Yang, *Adv. Energy Mater.* **2011**, *1*, 394.
- [22] Z. Wang, B. Huang, S. Wang, R. Xue, X. Huang, L. Chen, *Electrochim. Acta* **1997**, *42*, 2611.
- [23] L. M. Torell, P. Jacobsson, G. Petersen, *Polym. Adv. Technol.* **1993**, *4*, 152.
- [24] T. Caruso, S. Capoleoni, E. Cazzanelli, R. G. Agostino, P. Villano, S. Passerini, *Ionics* **2002**, *8*, 36.
- [25] Z. Peng, S. A. Freunberger, Y. Chen, P. G. Bruce, *Science* **2012**, *337*, 563.
- [26] D. Aurbach, E. Pollak, R. Elazari, G. Salitra, C. S. Kelley, J. Affinito, *J. Electrochem. Soc.* **2009**, *156*, A694.
- [27] a) X. Yu, A. Manthiram, *Phys. Chem. Chem. Phys.* **2015**, *17*, 2127; b) M. Cuisinier, C. Hart, M. Balasubramanian, A. Garsuch, L. F. Nazar, *Adv. Energy Mater.* **2015**, DOI: 10.1002/aenm.201401801.
- [28] A. Manthiram, Y. Fu, Y.-S. Su, *Acc. Chem. Res.* **2012**, *46*, 1125.
- [29] L. Suo, Y.-S. Hu, H. Li, M. Armand, L. Chen, *Nat. Commun.* **2013**, *4*, 1481.
- [30] X. Ji, L. F. Nazar, *J. Mater. Chem.* **2010**, *20*, 9821.
- [31] L. Yue, W. Li, F. Sun, L. Zhao, L. Xing, *Carbon* **2010**, *48*, 3079.
- [32] J. Zheng, M. Gu, M. J. Wagner, K. A. Hays, X. Li, P. Zuo, C. Wang, J.-G. Zhang, J. Liu, J. Xiao, *J. Electrochem. Soc.* **2013**, *160*, A1624.
- [33] R. A. Laudise, E. D. Kolb, A. J. Caporaso, *J. Am. Ceram. Soc.* **1964**, *47*, 9.